PROGRESS IN PHOTOVOLTAICS

Interface Engineering of Ultrathin Cu(In,Ga)Se2 Solar Cells on Reflective Back Contacts

Journal:	*Progress in Photovoltaics: Research and Applications*
Manuscript ID	PIP-20-108
Wiley - Manuscript type:	Research Article
Date Submitted by the Author:	07-Jun-2020
Complete List of Authors:	Gouillart, Louis; CNRS, C2N; IPVF, Cattoni, Andrea; CNRS, C2N Chen, Wei-Chao; Ångströmlaboratoriet, Engineering Sciences, Solid State Electronics Goffard, Julie; IPVF, Riekehr, Lars; Ångströmlaboratoriet, Engineering Sciences, Solid State Electronics Keller, Jan; Ångströmlaboratoriet, Engineering Sciences, Solid State Electronics Jubault, Marie; EDF R&D, IRDEP Naghavi, Negar; CNRS, IPVF, Edoff, Marika; Uppsala University, Department of Engineering Sciences Collin, Stéphane; CNRS, C2N; IPVF,
Keywords:	ultrathin solar cells, CIGS, silver, reflective back contact, interface engineering

Interface Engineering of Ultrathin Cu(In,Ga)Se_2 Solar Cells on Reflective Back Contacts

Louis Gouillart[1,2], Andrea Cattoni[1], Wei-Chao Chen[3], Julie Goffard[1], Lars Riekehr[3], Jan Keller[3], Marie Jubault[4], Negar Naghavi[2], Marika Edoff[3], Stéphane Collin[1,*]

[1]Centre for Nanoscience and Nanotechnology (C2N), CNRS, Université Paris-Saclay, 91120 Palaiseau, France

[2]IPVF UMR 9006, CNRS, 18 boulevard Thomas Gobert, 91120 Palaiseau, France

[3]Ångström Solar Centre, Division of Solid State Electronics, Uppsala University, PO Box 534, SE - 75121 Uppsala, Sweden

[4]EDF R&D, IPVF, 18 boulevard Thomas Gobert, 91120 Palaiseau, France

*corresponding author at: Centre for Nanoscience and Nanotechnology (C2N), CNRS, Université Paris-Saclay, 10, boulevard Thomas Gobert, 91120 Palaiseau, France.

E-mail address: stephane.collin@c2n.upsaclay.fr

Abstract

Cu(In,Ga)Se_2-based solar cells with ultrathin (<500 nm) absorber layers suffer from the low reflectivity of conventional Mo back contacts. Here, we design and investigate ohmic and reflective back contacts (RBC) made of multilayer stacks that are compatible with the direct deposition of CIGS at 500°C and above. Diffusion mechanisms and reactions at each interface and in the CIGS layer are carefully analyzed by EDX/STEM. It shows that the highly reflective silver mirror is efficiently encapsulated in ZnO:Al layers. The detrimental reaction between CIGS and the top In_2O_3:Sn (ITO) layer used for ohmic contact can be mitigated by adding a 3 nm-thick Al2O3 layer and by decreasing the CIGS co-evaporation temperature from 550°C to 500°C. It also improves the compositional grading of Ga toward the CIGS back interface, leading to increased open circuit voltage and fill factor. The best ultrathin CIGS solar cell on RBC exhibits an efficiency of 13.5% (+1.0% as compared to Mo) with a short-circuit current density of 28.9 mA/cm2 (+2.6 mA/cm2) enabled by double-pass absorption in the CIGS layer. RBC are easy to fabricate and could benefit other photovoltaic devices that require highly reflective and conductive contacts subject to high temperature processes.

Keywords: ultrathin solar cells; CIGS; silver; reflective back contact; interface engineering

1. Introduction

Cu(In,Ga)Se_2-based (CIGS) solar cells are one of the most promising thin-film photovoltaic technologies, with recent record efficiencies above 23% using typical CIGS absorber thicknesses of 2 – 3 µm [1]. However, the cost as well as the low and geographically limited extraction volume of In may potentially limit large scale industrialization of competitive CIGS modules [2], [3]. Hence, reducing the thickness of the CIGS layer to 500 nm or less is a promising way to maintain low costs for CIGS solar cells and modules thanks to a decreased consumption of elemental In and a shorter deposition time of CIGS [4], [5]. However, the benefits of thinning down the absorber go beyond economics and costs as it also reduces the pathway for electron/hole extraction. This leads to a

reduction in recombination losses in the bulk of the absorber, having a beneficial effect on both charge carrier collection and open-circuit voltage. Ultrathin solar cells would perform better than standard ones if maximal absorption could be maintained through efficient light trapping [6].

Today, state-of-the-art solar cells including an ultrathin CIGS absorber show a record efficiency of 15.2% [7], which is still far from the performances of devices with standard CIGS thicknesses. This record ultrathin solar cell was fabricated on a Mo back contact, with an optimized co-evaporation process of CIGS and a composition grading of Ga. However, the efficiency of ultrathin CIGS devices on Mo suffers from back contact recombination [8], and from insufficient light absorption in the CIGS layer [9], which respectively lead to poor open-circuit voltages (V_{OC}) and short-circuit current densities (J_{SC}). In order to achieve ultrathin CIGS solar cells with high efficiencies, advanced light management as well as interface passivation techniques are required [9].

As numerical calculations indicate that the integration of a highly reflective back mirror is a prerequisite for efficient light trapping in ultrathin solar cells [6], [10], various back contact architectures have been investigated in order to enhance absorption in ultrathin CIGS layers [9]–[14]. In addition, using a highly reflective back contact could increase not only the J_{SC} of the solar cells but also the reflection of infrared photons with energies below the bandgap of CIGS, resulting in a lower operating temperature of devices and an increased efficiency [15]–[17]. Avoiding high operating temperatures could improve the reliability of CIGS devices.

Though Ag, Cu, Au and Al are the most promising reflective metals to significantly improve light absorption in ultrathin CIGS solar cells, they are not compatible with the direct co-evaporation of CIGS [11], [18], [19]. Up to now, only a few architectures of reflective back contacts that include a metallic mirror and are compatible with the CIGS deposition were reported, such as a metal/Al_2O_3 bilayer with point contacts on Mo [20], and metallic mirrors encapsulated by transparent conducting oxides (TCO) [21]–[23]. Such architectures with TCO-based back contacts are promising as they

should be compatible with low-cost industrial processes, but also with back contact texturing strategies for additional light trapping in ultrathin CIGS layers [24].

However, the fabrication of high-efficiency solar cells on TCO back contacts remains challenging. In particular, it is necessary to prevent detrimental phenomena resulting from the co-evaporation of CIGS at temperatures higher than 450°C, such as:

- the formation of a detrimental Ga oxide layer at the CIGS/TCO back interface [25]–[29], which is promoted when an external supply of Na is used [30], [31];
- the diffusion of metallic elements from the back contact to the absorber [20], [23].

The approach proposed in this paper is to develop an ohmic and reflective back contact (RBC) made of a multilayer stack that is compatible with the direct co-evaporation of CIGS at temperatures above 500°C, and with back contact texturing strategies. This RBC is made of a reflective silver mirror encapsulated in ZnO:Al layers, and of a top layer of In_2O_3:Sn (ITO) as a back contact with CIGS. The addition of a 3 nm-thick alumina layer on top of the RBC was also studied, in order to hinder the detrimental formation of Ga oxide at the interface between CIGS and the TCO back contact [30].

Improving the fundamental understanding of the physicochemical properties of the interface between the RBC and CIGS is an absolute prerequisite to achieve high efficiency ultrathin solar cells. Therefore, the CIGS/RBC interface was thoroughly investigated by transmission electron microscopy in scanning mode (STEM) coupled with energy dispersive x-ray (EDX) spectroscopy. The CIGS composition grading close to its back interface was examined together with the diffusion and chemical reaction of elements from each layer. The performances of complete solar cells were then analyzed with regards to the CIGS growth conditions and interface with the RBC, and were also compared to numerical simulations. Thanks to this interfacial engineering, robust RBC enabling double-pass absorption in the CIGS layer were developed, and a 13.5%-efficient ultrathin solar cell was achieved with a short-circuit current density of J_{SC} = 28.9 mA/cm^2.

2. Methods

2.1. Sample fabrication

The ultrathin CIGS solar cells described in this study were prepared on 3 mm-thick soda-lime glass (SLG) substrates. Reference back contacts consist of a Mo layer deposited by DC-sputtering, with a thickness of 300 nm and a sheet resistance of R_{SH} = 0.6 Ω/sq. The RBC is composed of a stack of SLG (3 mm)/ZnO:Al (50 nm)/Ag (150 nm)/ZnO:Al (30 nm)/ITO (100 nm). The ZnO:Al and ITO layers were deposited by rf-sputtering, and Ag was deposited by electron beam evaporation. In addition, Ti adhesion layers were deposited by electron beam evaporation before and after the silver layer in order to promote adhesion at both interfaces. To keep the high reflectivity of silver, a thickness of 2 nm is chosen for the top Ti layer as a trade-off between adhesion and transparency. Half of the RBC samples were covered with a 3 nm-thick layer of Al_2O_3 made by atomic layer deposition at 200°C using trimethylaluminium and H_2O precursors (30 cycles). Prior to CIGS deposition, an 8 nm-thick precursor layer of NaF was deposited by thermal evaporation on each type of back contact. Ultrathin CIGS layers were then co-evaporated using a 3-stage process (Cu-poor, Cu-rich, Cu-poor) without any alkali post-deposition treatment. A composition grading of Ga was created by increasing the Ga and decreasing the In evaporation rates during the first deposition stage. In order to investigate the effects of the CIGS deposition temperature on its back interface with ITO, CIGS was co-evaporated in two separate runs, one with a standard maximum substrate temperature of 550°C and the other with a lower temperature of 500°C. For both CIGS layers, an average thickness of 510 nm was determined with a Dektak 150 stylus profilometer. Average atomic ratios of [Cu]/([Ga]+[In]) = 0.88 (CGI) and [Ga]/([Ga]+[In]) = 0.40 (GGI) were calculated from the x-ray fluorescence signal (XRF, Spectro X-Lab 2000) of CIGS on Mo references. Solar cells were completed with a standard stack of chemical bath deposited CdS (50 nm) and rf-sputtered i-ZnO/ZnO:Al (50 nm/250 nm) without a grid. Cells with an area of 0.1

cm² were separated by chemical etching of the CdS/i-ZnO/ZnO:Al stack after the deposition of a photolithography mask. The full solar cell stacks are depicted in Figure 1.

2.2. Characterization methods

The reflectance of the RBC stacks was determined with an Agilent Cary 5000 spectrophotometer equipped with an integrating sphere. Scanning electron microscopy (SEM, FEI Magellan 400L) was used to investigate the morphology of CIGS layers co-evaporated on Mo and RBC. The composition depth profiles of CIGS thin films on top of Mo and RBC were characterized by glow discharge optical emission spectroscopy (GD-OES, Spectruma Analytik GDA 750 HR). Note that CIGS/RBC samples studied by GD-OES originate from another batch of CIGS with identical nominal parameters for CIGS deposition. Thin cross-section lamellas of each CIGS sample grown on a RBC were prepared with a focused ion beam (FEI Strata DB235) and mounted to a Ti lift out grid. The lamellas were characterized with a probe corrected TEM (FEI Titan Themis), operated at 200 kV and equipped with the SuperX EDS system for EDX spectroscopy. EDX analysis was carried out in STEM mode and elemental maps were acquired with the Esprit 1.9 software from Bruker. Current-voltage (IV) characteristics and External Quantum Efficiencies (EQE) were measured with home-made setups. For each sample, the IV characteristics of 16 solar cells with an active area of 0.1 cm^2 were analyzed under dark and one-sun illumination. Light IV characteristics were determined with a halogen lamp resulting in a spectral mismatch with respect to the AM1.5G spectral irradiance. Hence, for each sample, the short-circuit current (J_{SC}) of the best cell was calculated from the EQE in order to correct the J_{SC} and efficiency values determined from light IV measurements.

2.3. Optical model

Light absorption in ultrathin CIGS solar cells with Mo and RBC were simulated with the RETICOLO software [32] based on the rigorous coupled wave analysis method. The optical indices

of CIGS were determined by ellipsometry, and the thickness of the simulated CIGS layers was fixed at its experimental average value of 510 nm. The optical indices of ITO were also derived from ellipsometry data described in a previous study [29]. More information about this optical model and the optical simulations performed in this study can be found in reference [10].

3. Results

3.1. Characterization of reflective back contacts

We first tested the optical properties and mechanical stability of the RBC stacks after high temperature treatments, before integrating them in the fabrication process of CIGS solar cells. Indeed, a mirror made of a single silver layer cannot sustain high temperatures without coalescence and diffusion into CIGS [19], which is why the silver layer of our RBC is encapsulated in ZnO:Al layers.

After a 10-minute annealing in air at a nominal temperature of 540°C, the RBC did not delaminate and its morphology did not exhibit any noticeable change. The reflectance of the RBC was analyzed before and after annealing, as can be seen in Figure 2. The RBC shows a much higher reflectance in air as compared to a standard Mo back contact. Besides, the annealing of the RBC resulted in a significant enhancement of the RBC reflectivity for wavelengths above 600 nm. This improvement is due to a modification of ITO optical indices upon annealing, as determined by ellipsometry in a previous study [29]. The annealed RBC reaches an average reflectance of 92.6% for wavelengths above 500 nm. These promising properties are expected to be maintained during the CIGS co-evaporation at temperatures close to 540°C.

Four point probes measurements were also carried out on the RBC, and respective sheet resistances of R_{SH} = 0.08 Ω/sq and 0.07 Ω/sq were measured before and after annealing. Thus, the RBC shows sufficient lateral conductivity, almost unchanged after annealing. A sheet resistance of R_{SH} = 45 Ω/sq was determined for a 200 nm-thick ITO layer on SLG, which indicates that the much

lower sheet resistances measured for the RBC is ensured by the Ag layer. As a result, the ITO layer on top of the RBC can be thinned or less conductive to limit parasitic light absorption in the infrared.

3.2. Characterization of ultrathin $Cu(In,Ga)Se_2$ layers co-evaporated at 550°C and 500°C

The CIGS deposition temperature has been reported to be a critical parameter in order to achieve an ohmic back contact with ITO [26], [27]. For this reason, CIGS layers co-evaporated at 550°C and 500°C were studied. We first detail the effects of temperature on the morphology and composition profile of CIGS.

Figure 3 compares SEM cross-section images of ultrathin CIGS layers co-evaporated on Mo and RBC for substrate temperatures of 550°C and 500°C. It reveals that large and columnar CIGS grains are grown at 550°C on Mo while smaller CIGS grains are formed at 500°C, as expected with a lower deposition temperature [33]. The observed CIGS grains are smaller when CIGS is deposited on top of the RBC, and similarly to the case of a Mo back contact their size also decreases for a co-evaporation temperature of 500°C. Besides, the ITO layer of the RBC appears to be rough when CIGS is co-evaporated at 550°C, while a smooth CIGS/ITO interface and rectangular ITO grains are obtained for a CIGS deposition temperature of 500°C. To have a better understanding of the interface between the CIGS layer and the RBC, the composition profiles of these samples were analyzed by GD-OES.

CGI and GGI depth profiles of CIGS layers deposited at 550°C or 500°C were determined by GD-OES, as shown in Figure 4. The CGI depth profiles are found to be constant both for Mo and RBC. In contrast, graded GGI compositions are observed on Mo back contacts, with a steeper profile when the CIGS deposition temperature is decreased from 550°C to 500°C (Figures 4a and 4b). An increasing GGI ratio at the back interface of CIGS is known to create a back surface field that repels electrons toward the front interface [7]. Hence, the deposition of ultrathin CIGS at 500°C

and subsequent steeper GGI back grading should improve the rear passivation of CIGS. The GGI depth profiles of ultrathin CIGS layers grown on RBC seem to be quite flat through the bulk of the CIGS, with an increase only near the back contact (Figures 4c and 4d). This GGI back grading is also steeper when CIGS is co-evaporated on the RBC at 500°C instead of 550°C, similarly to the case of a Mo back contact.

Because of the limited depth resolution of the GD-OES, it is difficult to assess the evolution of the composition at the CIGS/ITO interface. This is why a STEM/EDX study was carried out in order to further investigate the interface between the CIGS layer and the RBC.

3.3. STEM/EDX analysis of the Cu(In,Ga)Se_2/reflective back contact interfaces

An extensive STEM/EDX study of CIGS layers deposited on RBC was conducted, and the stability of the RBC and its interface with CIGS were analyzed. Figure 5a presents a high angle annular dark field (HAADF) STEM image of a complete CIGS solar cell prepared at 550°C on a RBC, along with the corresponding EDX maps of absorber elements as well as Cd, O, Zn, Ag and GGI. The RBC stack appears to be stable under CIGS deposition conditions, but an accumulation of Ga is visible at the interface of CIGS with the RBC. In order to investigate the RBC region in detail, a STEM/EDX analysis of higher magnification was also conducted closer to the back interface of CIGS.

In this study four CIGS/RBC interfaces are compared: CIGS layers co-evaporated at 550°C and 500°C on a bare RBC and a RBC covered with a 3 nm-thick Al_2O_3 layer. For each sample, Figures 5b to 5e show the STEM HAADF image with its associated EDX mappings.

Independently of the deposition temperature, a small portion of Ag is observed in the ZnO:Al layer and at the bottom of the ITO layer. This is attributed to the oxidation of silver, and the expansion of silver oxide during the transfer of the lamellas from the FIB to the TEM vacuum chamber, as confirmed by the significant detection of O in the Ag layer (Figure 5). With similar

stacks and CIGS deposition processes, we have checked that silver is not detected outside the deposited layer when a quick transfer between the FIB and STEM/EDX tools is performed (not shown). ZnO:Al acts as an effective blocking layer for the diffusion of Ag through the absorber. On the other hand, the CIGS/ITO interface region shows an accumulation of Ga that is found to be stronger for absorbers deposited at 550°C rather than 500°C (Figures 5b and 5c). Based on EDX mappings, the increased Ga signal has been attributed to the formation of Ga oxide, as the enrichment in Ga matches the presence of O and the depletion of elemental Cu, In and Se.

Figures 5d and 5e reveal that regardless of the CIGS deposition temperature, adding a 3 nm-thick Al_2O_3 layer on the RBC stack does not prevent the growth of a Ga oxide layer, but strongly reduces its roughness as compared to a bare RBC, for which the Ga oxide phase also extends into ITO grain boundaries. In addition, for CIGS/Al_2O_3/ITO samples the Ga and Al signals are overlapped at the back interface of CIGS, possibly because of the formation of a $(Al_xGa_{1-x})_2O_3$ alloy [34], [35]. It is also worth mentioning that when the RBC is covered with alumina and the CIGS layer is co-evaporated at 500°C, CIGS is observed in the ITO grain boundaries rather than Ga oxide, as confirmed in particular by the depletion of O (Figure 5e).

The average GGI depth profiles were also calculated from the STEM/EDX data for each CIGS deposition temperature and RBC (Figure 6). As in the GD-OES analysis (Figure 4), the GGI back grading is steeper when the CIGS deposition temperature is decreased from 550°C to 500°C. Besides, the formation of Ga oxide is distinguished by a GGI peak at the CIGS/ITO interface. It confirms that less Ga oxide is formed when the CIGS layer is deposited at 500°C instead of 550°C, and that the Ga oxide layer grown at 550°C is thinner when the RBC is covered by a 3 nm-thick Al_2O_3 layer.

3.4. Photovoltaic performances of ultrathin Cu(In,Ga)Se_2 solar cells

Complete ultrathin solar cells were fabricated by co-evaporation of CIGS with deposition temperatures of 550°C and 500°C on Mo as well as RBC with and without a 3 nm-thick top layer of alumina. Their photovoltaic performances were measured, and are summarized in Table 1. The IV characteristics and EQE curves of the best cells are presented in Figure 7.

In the case of a Mo back contact, decreasing the CIGS deposition temperature from 550°C to 500°C leads to an increase in average efficiency from 9.5 ± 0.6 % to 12.4 ± 0.1 %, thanks to V_{OC} and fill factor (*FF*) improvements from 568 ± 10 mV to 630 ± 4 mV and from 64.6 ± 2.9 % to 75.0 ± 0.5 %, respectively. This is attributed to the steeper GGI back grading that is formed when CIGS is deposited at 500°C, creating a back surface field that helps to passivate the rear interface of CIGS. Consistently, the dark saturation current densities extracted from the dark IV characteristics with a one-diode model are found to decrease with the reduction of the CIGS deposition temperature (Table S1).

Co-evaporating CIGS at 550°C on a bare RBC results in the degradation of all IV parameters. This is due to the formation of a thick and rough Ga oxide layer at the back interface of CIGS with ITO, which depletes the CIGS layer of Ga and leads to a flat GGI profile and conduction band. Still, the co-evaporation of CIGS at 500°C rather than 550°C improves the V_{OC}, *FF* and efficiency of cells with RBC, thanks to the lower amount of Ga oxide and the subsequent steeper GGI back grading that creates a passivating back surface field. When CIGS is deposited at 500°C on a RBC with 3 nm of Al_2O_3, the formation of a thin and smooth Ga oxide layer as well as a possible passivation effect of alumina lead to a best cell efficiency of 13.5% with a V_{OC} of 644 mV and a *FF* of 72.7%. In comparison, CIGS solar cells fabricated at 550°C on a RBC covered with alumina exhibit a lower efficiency of 11.2%, with a V_{OC} of 595 mV and a *FF* of 68.5%.

The best cell efficiency was successfully improved by replacing Mo with a RBC. This efficiency enhancement is mostly related to the higher J_{SC} of 28.9 mA/cm^2 in the case of a RBC, instead of 26.2 mA/cm^2 for the Mo reference. However, the best average V_{OC} and *FF* were achieved with a CIGS layer co-evaporated at 500°C on Mo. In particular, the *FF* of solar cells fabricated on

bare RBC show a large spread, in correlation with a voltage-dependent photocurrent. When the RBC are covered with 3 nm of alumina, the voltage-dependence of the best cells photocurrent is mitigated (Figure 7) and the average *FF* are improved regardless of the co-evaporation temperature. Besides, the addition of alumina on ITO dramatically improves the photovoltaic performance of cells fabricated at 550°C. These beneficial effects of the alumina layer are attributed to the rear passivation of the CIGS layer, which could be due to the growth of a smoother Ga oxide layer at the CIGS back interface and/or a chemical passivation thanks to a reduced interface defects density. Nevertheless, the best cell prepared at 500°C on Mo exhibits a *FF* of 75.8%, as compared to 72.7% in the case of a RBC with alumina. This slight *FF* loss is due to an increase of the series resistance (see Supplementary Information), which is expected for alumina layers thicker than 1.5 nm [36]. A sufficient current conduction is still achieved, and can be attributed to the presence of openings in the Al_2O_3 layer [37].

It is worth mentioning that in several previous studies, the presence of a Ga oxide layer at the CIGS back contact was shown to be detrimental to cell performances because of an increase of the series resistance and a current blocking behavior [21], [26], [27], [38], [39]. In this work however, the growth of a thick and rough Ga oxide layer led to a depletion of Ga in the CIGS layer close to its back contact, which results in a decreased V_{OC} and a voltage-dependent photocurrent.

The EQE of the best solar cells (Figure 7) indicate that the J_{SC} improvement enabled by the RBC is related to large resonances at wavelengths above 650 nm. Figure 8 shows the simulated optical absorption in each layer of the complete CIGS solar cells prepared at 500°C on Mo and RBC. While the simulated CIGS absorption matches well the experimental EQE of the solar cell with a RBC, the discrepancies observed in the case of a Mo back contact are attributed to variations of the thicknesses of the solar cell layers. The simulated absorption spectra demonstrate that the substantial absorption losses in Mo (gray area in Figure 8) can be avoided by enhancing the CIGS back reflectance with a RBC, which in turn increases light absorption in CIGS.

From our results, the current density improvement indicates that the RBC is stable up to a temperature of at least 500°C, which should be sufficient to obtain highly efficient cells [40]. Hence, ultrathin CIGS solar cells on RBC still have room for improvement, especially regarding the optimization of the Ga profile. An optimized composition profile in the CIGS layer that compensates for losses attributed to the Ga oxide formation, in combination with an efficient passivation of the back contact, may reduce the electrical losses at the back contact and increase both the V_{OC} and *FF*. In addition, the incorporation of NaF via a post-deposition treatment rather than a precursor layer should further reduce the growth of Ga oxide [30], [31], and is thus expected to be beneficial for cell performances.

4. Conclusion

In this work, we have developed a highly reflective back contact (RBC) made of a multi-layer stack that includes a silver mirror and a top layer of ITO. This RBC is suitable for the direct fabrication of CIGS solar cells as it was shown to meet two essential requirements: it can withstand the high deposition temperatures (≥ 500°C) of CIGS, while also forming an ohmic contact with the absorber. Replacing Mo with a RBC leads to a significant EQE enhancement, and the best ultrathin cell with a RBC and a 510 nm-thick CIGS layer exhibits a short-circuit current density of J_{SC} = 28.9 mA/cm^2 and an efficiency of η = 13.5%, which are 2.6 mA/cm^2 and 1.0% absolute more, respectively, than with a Mo back contact. The optical simulations of complete solar cells are in good agreement with the experimental EQE. Light absorption simulations also indicate that enhancing the CIGS back reflectance with a RBC avoids substantial absorption losses in Mo, resulting in an increased CIGS light absorption.

In order to increase the V_{OC} and *FF* of CIGS solar cells including a RBC, we have shown that it is necessary to adjust the deposition temperature of CIGS and to improve the back interface of CIGS with ITO. When CIGS is co-evaporated at 550°C on a bare RBC, the formation of a thick and

rough Ga oxide layer at the interface between CIGS and ITO was detected by STEM/EDX, and was found to be detrimental to the cell performance. It was possible to reduce the roughness of Ga oxide by adding a 3 nm-thick layer of Al_2O_3 between the CIGS and ITO layers. Covering the RBC with this thin alumina layer may also contribute to the CIGS rear passivation, as indicated by the lower voltage-dependence of the photocurrent. Importantly, decreasing the CIGS deposition temperature from 550°C to 500°C efficiently mitigates the growth of Ga oxide at the CIGS/ITO interface. It also leads to a steeper GGI grading both for Mo and RBC, which creates a beneficial back surface field within the CIGS layer. As a result, the co-evaporation of CIGS at 500°C and the deposition of an additional 3 nm-thick alumina layer on the RBC successfully led to V_{OC} and *FF* values close to the ones of the Mo reference. An optimization of the CIGS rear passivation, GGI grading as well as Na incorporation should further improve the V_{OC} and *FF* of devices including a RBC.

To conclude, the RBC presented here is compatible with the high deposition temperature of CIGS absorbers and exhibits a high reflectivity enabling double-pass absorption in the CIGS layer. It allows a decrease of the CIGS thickness by a factor of two with no J_{SC} loss, while maintaining similar V_{OC} and *FF* values as compared to the conventional Mo back contact. With an additional anti reflection coating, a J_{SC} above 30 mA/cm^2 is expected for 500 nm-thick CIGS layers. This work also paves the way toward the fabrication of a nanostructured RBC that can further improve light trapping in ultrathin solar cells, as proposed recently in CIGS [10], [24] and GaAs [6] solar cells with nanostructured back mirrors.

Acknowledgments

This work was supported by the ARCIGS-M Project, as part of the European Union's Horizon 2020 Research and Innovation Program under Grant 720887.

List of figures

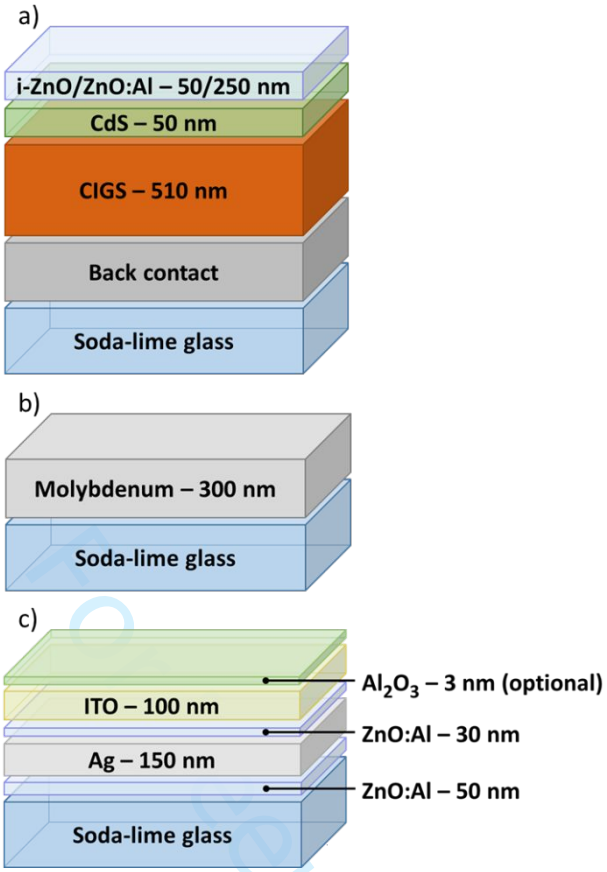

1. Schematic of a) the fabricated ultrathin CIGS solar cells, with detailed back contact architectures consisting of b) Mo and c) RBC with and without an additional alumina layer.

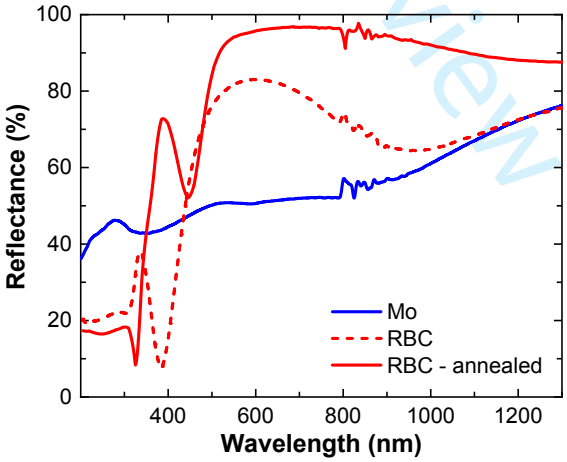

2. Reflectance in air of 600 nm-thick molybdenum (blue) and RBC (red), before and after annealing in air at 540°C for 10 minutes (dashed and solid lines, respectively).

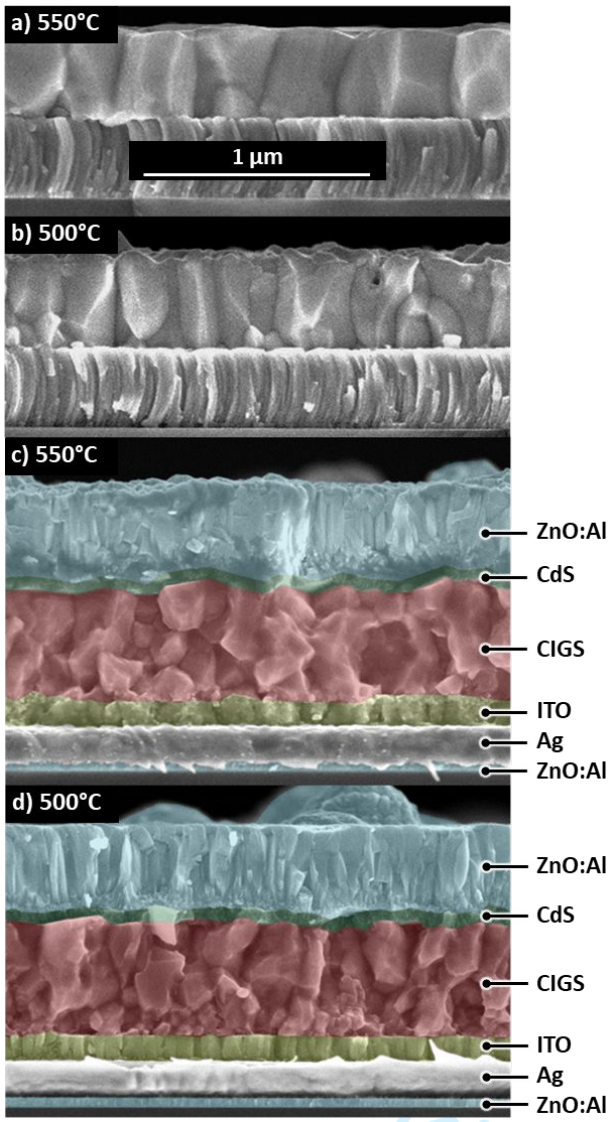

3. Scanning electron microscopy (SEM) cross-section images of ultrathin CIGS layers co-evaporated on Mo at a) 550°C and b) 500°C, together with cross-sections images of complete ultrathin CIGS solar cells prepared at c) 550°C and d) 500°C on a RBC.

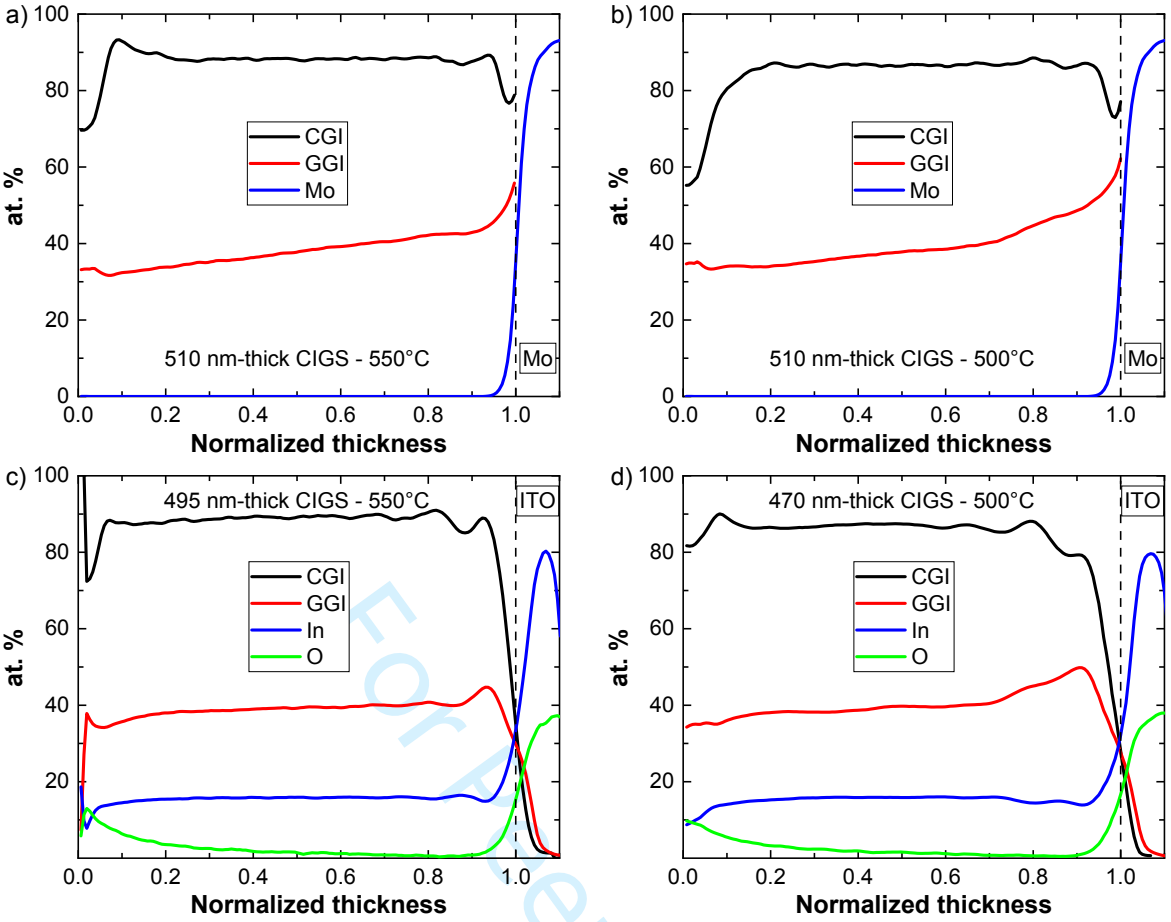

4. Profiles of [Cu]/([Ga]+[In]) and [Ga]/([Ga]+[In]) atomic ratios (respectively CGI and GGI) determined by GD-OES. CIGS was co-evaporated on molybdenum and RBC at a,c) 550°C and b,d) 500°C. GD-OES signal was calibrated with average atomic compositions measured in XRF, and CIGS thicknesses were measured with a profilometer. Vertical dashed lines indicate the back interface of the CIGS layer.

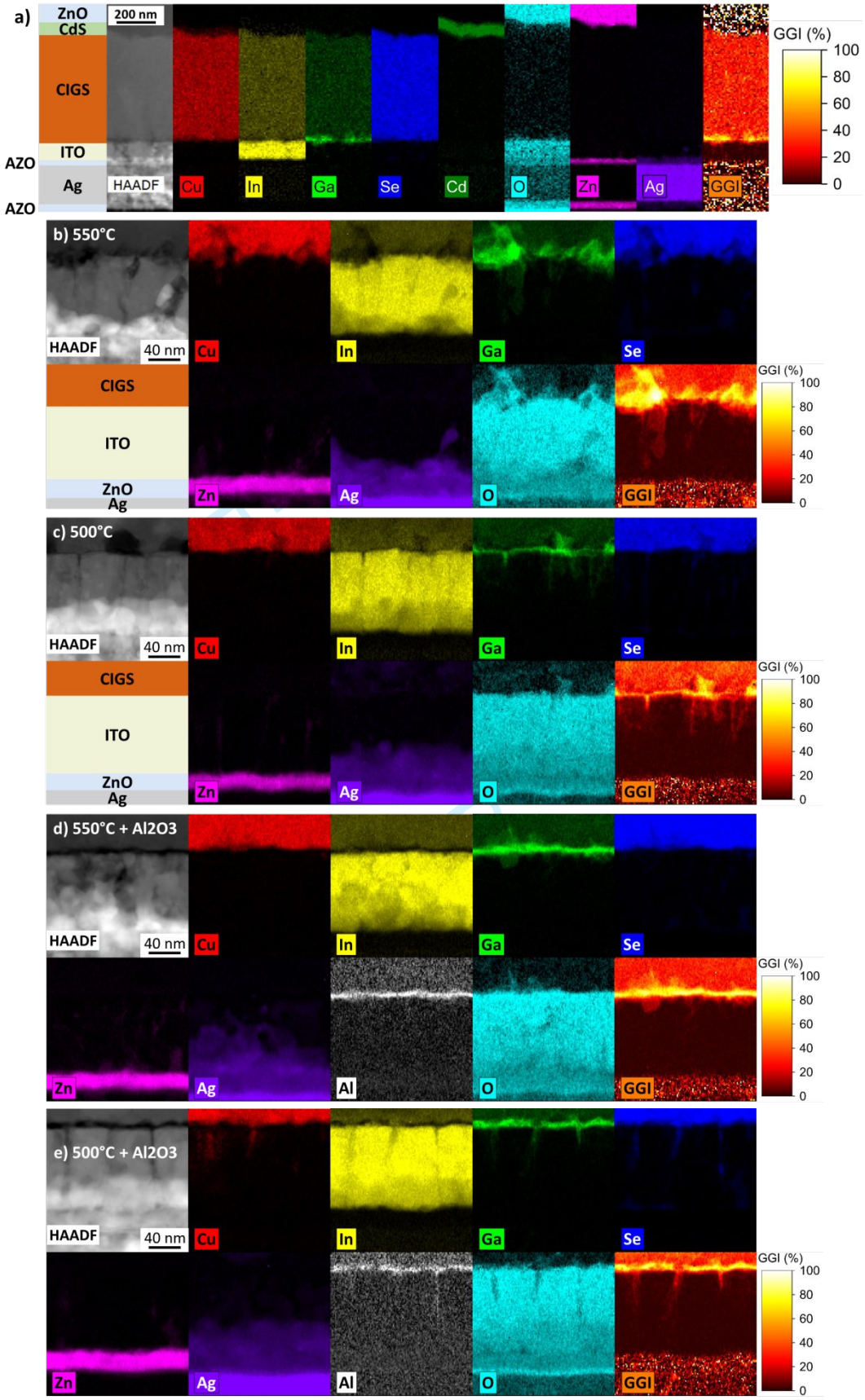

5. HAADF images and corresponding STEM/EDX maps of CIGS layers co-evaporated on RBC. CIGS was co-evaporated at a,b,d) 550°C and c,e) 500°C. In d) and e), the RBC was covered with a 3 nm-thick alumina layer prepared by ALD. For the sake of clarity, schematics of the observed layers are also shown in a), b) and c).

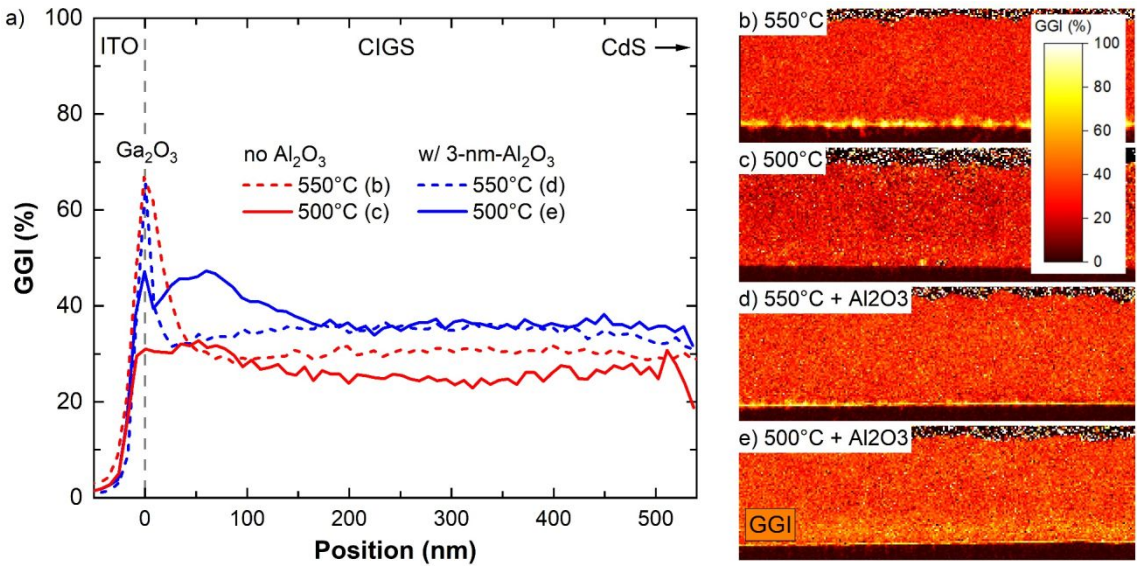

6. a) Average GGI depth profiles of ultrathin CIGS layers on RBC, determined from b-e) their STEM/EDX maps of the GGI ratio. CIGS was co-evaporated at either b,d) 550°C or c,e) 500°C, on b,c) bare RBC and d,e) RBC covered with 3 nm-thick Al_2O_3 layers.

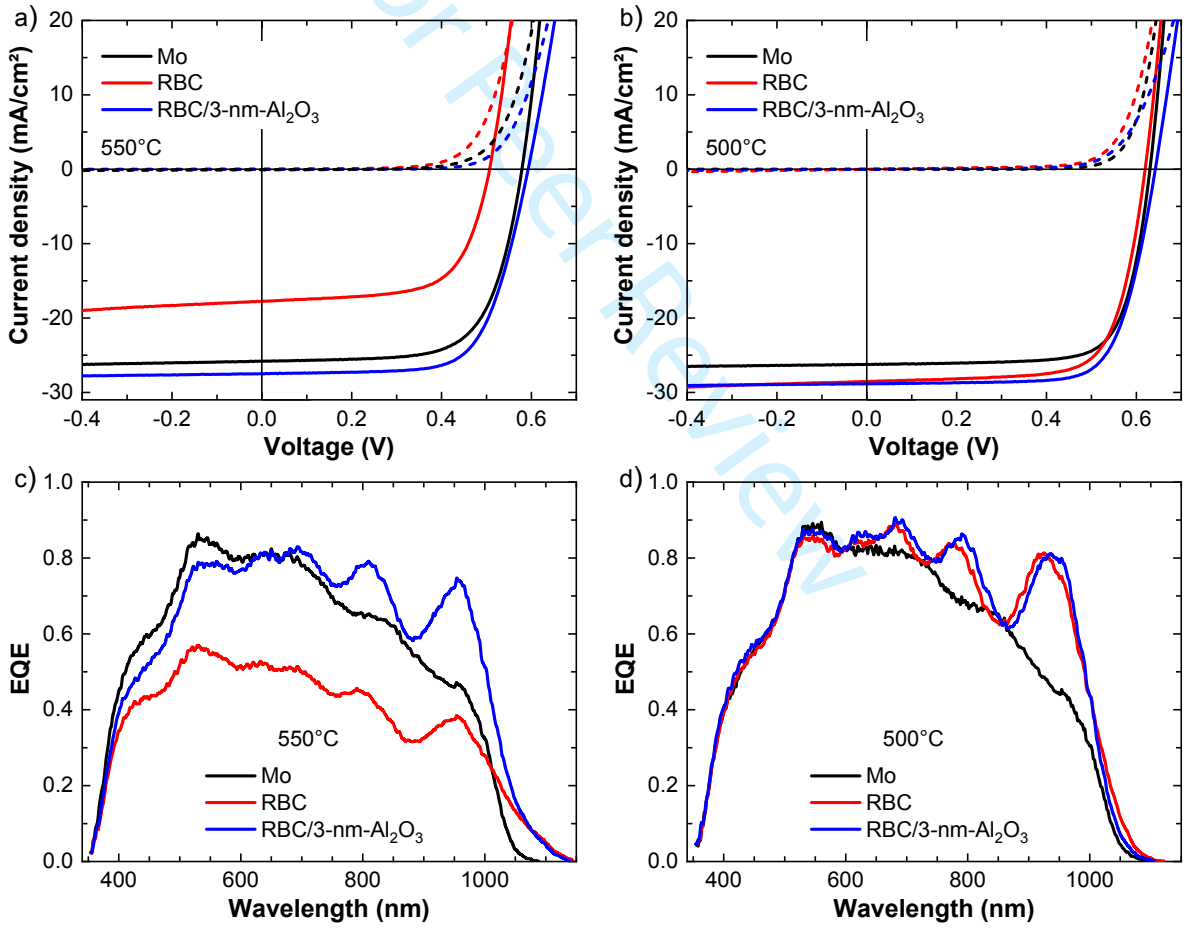

7. a,b) IV characteristics under one-sun illumination (solid lines) and in the dark (dashed lines), as well as c,d) EQE of best ultrathin solar cells. CIGS layers were co-evaporated at a,c) 550°C and b,d) 500°C, with back contacts made of Mo (black), RBC (red) and RBC covered with a 3 nm-thick Al_2O_3 layer (blue).

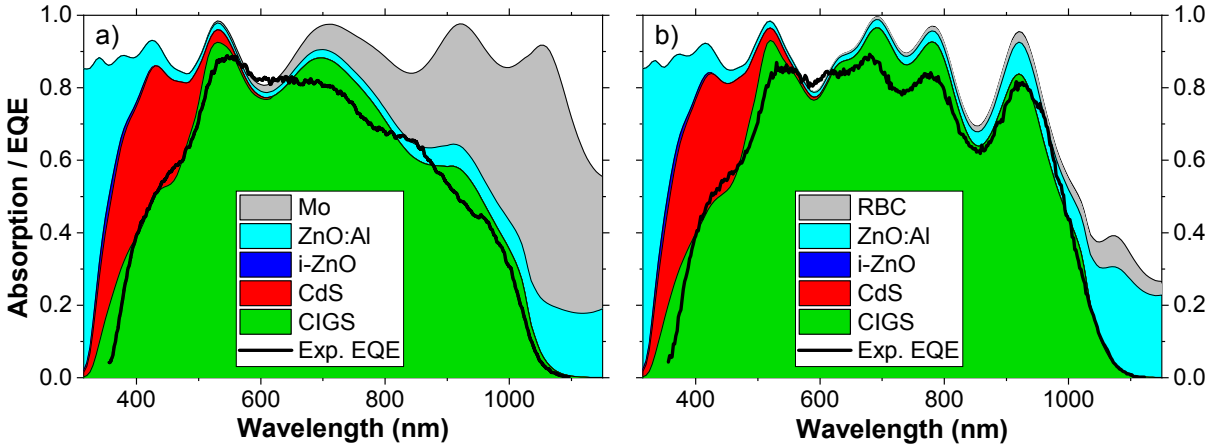

8. Simulated absorption under AM1.5G illumination, for each layer of experimental ultrathin solar cells on a) molybdenum and b) RBC. CIGS was co-evaporated at 500°C. The respective experimental EQE curves are also shown for comparison.

	Back-contact	Eff. (%)	J_{SC} (EQE) (mA/cm²)	V_{OC} (mV)	FF (%)
CIGS – 550°C	Mo	9.5 ± 0.6 / 10.2	25.8	568 ± 10 / 582	64.6 ± 2.9 / 68.2
	RBC	4.3 ± 1.2 / 5.9	17.8	452 ± 60 / 510	53.9 ± 9.1/ 65.7
	RBC/3-nm-Al_2O_3	9.9 ± 1.1 / 11.2	27.5	581 ± 15 / 595	62.0 ± 6.2 / 68.5
CIGS – 500°C	Mo	12.4 ± 0.1 / 12.5	26.2	630 ± 4 / 635	75.0 ± 0.5 / 75.8
	RBC	11.4 ± 1.2 / 12.8	28.5	611 ± 16 / 620	65.5 ± 5.5 / 72.3
	RBC/3-nm-Al_2O_3	12.3 ± 1.0 / 13.5	28.9	618 ± 15 / 644	68.8 ± 3.8 / 72.7

Table 1. Light IV parameters for CIGS co-evaporation temperatures of 550°C and 500°C. Back contacts consist of Mo, as well as RBC with and without a 3 nm-thick alumina layer on top. Average values with standard deviation were derived from the 10 best solar cells except for J_{SC}, which were calculated from the EQE of the corresponding best solar cells.

References

[1] M. Nakamura, K. Yamaguchi, Y. Kimoto, Y. Yasaki, T. Kato, and H. Sugimoto, "Cd-Free Cu(In,Ga)(Se,S)$_2$ Thin-Film Solar Cell With Record Efficiency of 23.35%," *IEEE J. Photovolt.*, **2019**, *9*, 1863.

[2] European Commission, *Report on Critical Raw Materials in the Circular Economy*. **2018**.

[3] Government Publishing Office, *Mineral Commodities Summary 2018*. U S Govt. Printing Office, **2018**.

[4] M. Edoff, S. Schleussner, E. Wallin, and O. Lundberg, "Technological and economical aspects on the influence of reduced Cu(In,Ga)Se2 thickness and Ga grading for co-evaporated Cu(In,Ga)Se2 modules," *Thin Solid Films*, **2011**, *519*, 7530.

[5] K. A. W. Horowitz, R. Fu, and M. Woodhouse, "An analysis of glass–glass CIGS manufacturing costs", *Solar Energy Materials and Solar Cells*, **2016**, *154*, 1–10.

[6] H.-L. Chen *et al.*, "A 19.9%-efficient ultrathin solar cell based on a 205-nm-thick GaAs absorber and a silver nanostructured back mirror," *Nat. Energy*, **2019**, *4*, 761-767.

[7] L. M. Mansfield *et al.*, "Efficiency increased to 15.2% for ultra-thin Cu(In,Ga)Se $_2$ solar cells," *Prog. Photovolt. Res. Appl.*, **2018**, *26*, 949-954.

[8] P. M. P. Salomé *et al.*, "Passivation of Interfaces in Thin Film Solar Cells: Understanding the Effects of a Nanostructured Rear Point Contact Layer," *Adv. Mater. Interfaces*, **2018**, *5*, 1701101.

[9] N. Naghavi *et al.*, "Ultrathin Cu(In,Ga)Se2 based solar cells," *Thin Solid Films*, **2017**, *633*, 55-60.

[10] J. Goffard *et al.*, "Light Trapping in Ultrathin CIGS Solar Cells with Nanostructured Back Mirrors," *IEEE J. Photovolt.*, **2017**, *7*, 1433-1441.

[11] Z. J. Li-Kao *et al.*, "Towards ultrathin copper indium gallium diselenide solar cells: proof of concept study by chemical etching and gold back contact engineering," *Prog. Photovolt. Res. Appl.*, **2012**, *20*, 582-587.

[12] J. Malmström, S. Schleussner, and L. Stolt, "Enhanced back reflectance and quantum efficiency in Cu(In,Ga)Se2 thin film solar cells with a ZrN back reflector," *Appl. Phys. Lett.*, **2004**, *85*, 2634-2636.

[13] N. Dahan, Z. Jehl, J. F. Guillemoles, D. Lincot, N. Naghavi, and J.-J. Greffet, "Using radiative transfer equation to model absorption by thin Cu(In,Ga)Se2 solar cells with Lambertian back reflector," *Opt. Express*, **2013**, *21*, 2563.

[14] C. van Lare, G. Yin, A. Polman, and M. Schmid, "Light Coupling and Trapping in Ultrathin Cu(In,Ga)Se2 Solar Cells Using Dielectric Scattering Patterns," *ACS Nano*, **2015**, *9*, 9603–9613.

[15] K. Mullaney, G. M. Jones, C. A. Kitchen, and D. P. Jones, "Infra-red reflective coverglasses: the next generation," in *Conference Record of the Twenty Third IEEE Photovoltaic Specialists Conference - 1993 (Cat. No.93CH3283-9)*, **1993**, 1363–1368.

[16] W. Li, Y. Shi, K. Chen, L. Zhu, and S. Fan, "A Comprehensive Photonic Approach for Solar Cell Cooling," *ACS Photonics*, **2017**, *4*, 774–782.

[17] O. Dupré, R. Vaillon, and M. A. Green, "Physics of the temperature coefficients of solar cells," *Sol. Energy Mater. Sol. Cells*, **2015**, *140*, 92–100.

[18] N. Dahan *et al.*, "Optical approaches to improve the photocurrent generation in Cu(In,Ga)Se2 solar cells with absorber thicknesses down to 0.5 µm," *J. Appl. Phys.*, **2012**, *112*, 094902.

[19] K. Orgassa, H. W. Schock, and J. H. Werner, "Alternative back contact materials for thin film Cu(In,Ga)Se2 solar cells," *Thin Solid Films*, **2003**, *431–432*, 387–391.

[20] T. S. Lopes *et al.*, "Rear Optical Reflection and Passivation Using a Nanopatterned Metal/Dielectric Structure in Thin-Film Solar Cells," *IEEE J. Photovolt.*, **2019**, *9*, 1421–1427.

[21] B. Bissig *et al.*, "Novel back contact reflector for high efficiency and double-graded Cu(In,Ga)Se2 thin-film solar cells," *Prog. Photovolt. Res. Appl.*, **2018**, *26*, 894–900.

[22] T. Schneider and R. Scheer, "Aluminium Based Back Reflectors for Ultrathin Cu(In,Ga)Se2 Solar Cells with ITO Diffusion Barrier," presented at the 36th European Photovoltaic Solar Energy Conference and Exhibition (EU-PVSEC), Marseille, France, **2019**, pp. 684–688.

[23] L. Gouillart *et al.*, "Reflective Back Contacts for Ultrathin Cu(In,Ga)Se2-Based Solar Cells," *IEEE J. Photovolt.*, **2020**, *10*, 250-254.

[24] G. Yin, M. W. Knight, M.-C. van Lare, M. M. Solà Garcia, A. Polman, and M. Schmid, "Optoelectronic Enhancement of Ultrathin CuIn 1-x Ga x Se2 Solar Cells by Nanophotonic Contacts," *Adv. Opt. Mater.*, **2017**, *5*, 1600637.

[25] M. Terheggen, H. Heinrich, and G. Kostorz, "Ga_2O_3 segregation in Cu(In,Ga)Se2/ZnO superstrate solar cells and its impact on their photovoltaic properties," *Thin Solid Films*, **2002**, *403–404*, 212-215.

[26] T. Nakada, Y. Hirabayashi, T. Tokado, D. Ohmori, and T. Mise, "Novel device structure for Cu(In,Ga)Se2 thin film solar cells using transparent conducting oxide back and front contacts," *Sol. Energy*, **2004**, *77*, 739–747.
[27] T. Nakada, "Microstructural and diffusion properties of CIGS thin film solar cells fabricated using transparent conducting oxide back contacts," *Thin Solid Films*, **2005**, *480–481*, 419–425.
[28] H. Simchi, J. Larsen, K. Kim, and W. Shafarman, "Improved Performance of Ultrathin Cu(InGa)Se2 Solar Cells With a Backwall Superstrate Configuration," *IEEE J. Photovolt.*, **2014**, *4*, 1630–1635.
[29] L. Gouillart *et al.*, "Development of reflective back contacts for high-efficiency ultrathin Cu(In,Ga)Se2 solar cells," *Thin Solid Films*, **2019**, *672*, 1–6.
[30] J. Keller, W.-C. Chen, L. Riekehr, T. Kubart, T. Törndahl, and M. Edoff, "Bifacial Cu(In,Ga)Se2 solar cells using hydrogen-doped In2O3 films as a transparent back contact," *Prog. Photovolt. Res. Appl.*, **2018**, *26*, *846–858*.
[31] M. D. Heinemann *et al.*, "Cu(In,Ga)Se2 superstrate solar cells: prospects and limitations," *Prog. Photovolt. Res. Appl.*, **2015**, *23*, 1228–1237.
[32] P. Lalanne and J. P. Hugonin, "Reticolo software for grating analysis." [Online]. Available: https://www.lp2n.institutoptique.fr/lp2n/Membres-Services/Responsables-d-equipe/LALANNE-Philippe.
[33] T. Klinkert, M. Jubault, F. Donsanti, D. Lincot, and J.-F. Guillemoles, "Ga gradients in Cu(In,Ga)Se2: Formation, characterization, and consequences," *J. Renew. Sustain. Energy*, **2014**, *6*, 011403.
[34] V. G. Hill, R. Roy, and E. F. Osborn, "The System Alumina-Gallia-Water," *J. Am. Ceram. Soc.*, **1952**, *35*, 135–142.
[35] H. Peelaers, J. B. Varley, J. S. Speck, and C. G. Van de Walle, "Structural and electronic properties of Ga2O3-Al2O3 alloys," *Appl. Phys. Lett.*, **2018**, *112*, 242101.
[36] J. Keller, F. Gustavsson, L. Stolt, M. Edoff, and T. Törndahl, "On the beneficial effect of Al2O3 front contact passivation in Cu(In,Ga)Se2 solar cells," *Sol. Energy Mater. Sol. Cells*, **2017**, *159*, 189–196.
[37] D. Ledinek, O. Donzel-Gargand, M. Sköld, J. Keller, and M. Edoff, "Effect of different Na supply methods on thin Cu(In,Ga)Se2 solar cells with Al2O3 rear passivation layers," *Sol. Energy Mater. Sol. Cells*, **2018**, *187*, 160–169.
[38] J. K. Larsen, P. Xin, and W. N. Shafarman, "Formation of Ga2O3 barrier layer in Cu(InGa)Se2 superstrate devices with ZnO buffer layer," *MRS Proc.*, **2013**, *1538*, 67–72.
[39] Y.-S. Son *et al.*, "Control of Structural and Electrical Properties of Indium Tin Oxide (ITO)/Cu(In,Ga)Se2 Interface for Transparent Back-Contact Applications," *J. Phys. Chem. C*, **2019**, *123*, 1635–1644.
[40] R. Carron *et al.*, "Advanced Alkali Treatments for High-Efficiency Cu(In,Ga)Se2 Solar Cells on Flexible Substrates," *Adv. Energy Mater.*, **2019**, *9*, 1900408.